Stepped Spillway Prototype Operation and Air Entrainment: Toward a Better Understanding of the Mechanisms Leading to Air Entrainment in Skimming Flows

Hubert Chanson[1]

Abstract: A spillway is a conveyance structure designed to pass flood waters. The construction of steps down the steep chute may contribute to some energy dissipation, in turn reducing the size of the downstream energy dissipator. A unique opportunity for field observations was provided at the Hinze Dam Stage 3 (Gold Coast, Australia) between 2013 and 2021. Detailed observations were conducted for six overflow discharges within $20.9\ \mathrm{m^3/s} < Q < 334\ \mathrm{m^3/s}$ with Q the volume discharge, corresponding to dimensionless discharges $0.44 < d_c/h < 2.82$ with d_c the critical depth and h the step height and Reynolds numbers ranging from 0.68×10^7 to 10.8×10^7. Some uniquely novel aspects of the research included a series of systematic observations of a full-scale prototype stepped spillway, operating with a relatively wide range of unit discharges $1.71\ \mathrm{m^2/s} < q < 27.3\ \mathrm{m^2/s}$ with q the unit discharge. The observations provided new information on the basic hydraulic flow patterns, inception of free-surface aeration, and surface velocity field. Overall, the current study detailed some unique insights into the mechanisms leading to air entrainment in skimming flows in high-velocity prototype stepped spillways. While surface velocity measurements were achieved, the limitations are discussed and future enhancements are proposed. **DOI: 10.1061/(ASCE)HY.1943-7900.0002015.** © *2022 American Society of Civil Engineers.*

Author keywords: Dam spillways; Hinze Dam stepped spillway; Prototype operation; Inception point; Optical flow; Cavity ejection; Surface velocity field; Air entrapment mechanisms; Air-water surface features; Turbulence.

Introduction

A dam spillway is a structure designed to safely pass flood waters and dissipate their turbulent kinetic energy (Novak et al. 1996; Vischer and Hager 1998). Most dams are equipped with an overflow spillway, which typically includes a crest, steep chute and energy dissipator (USBR 1965). The incorporation of steps down the steep chute may contribute to some energy dissipation (Sorensen 1985; Chanson 1995). During a spill, the steps induce flow separation at the step edges, with very intense turbulent dissipation, leading to a significant reduction of kinetic energy at the downstream end of the steep stepped chute, as well as some strong self-aeration (Rajaratnam 1990; Chanson 2001; Boes and Hager 2003). A stepped chute may experience three distinctly different flow regimes depending upon the discharge, for a given step geometry (Ohtsu and Yasuda 1997; Chanson et al. 2015). At small discharges, the overflow consists of a series of free-falling nappes, impacting on the horizontal face of the downstream steps. A pseudochaotic motion with large hydrodynamic instabilities, spray and splashing is observed for a range of intermediate discharges (i.e., a transition flow). On a steep stepped spillway operating at a relatively large flow, the waters skim over the pseudobottom formed by step edges and form losses take place as momentum is transferred from the mainstream to the recirculation cavity flow (Rajaratnam 1990; Chanson et al. 2002; Zabaleta et al. 2020).

During the last four decades, research into the hydraulics of stepped spillways has been active worldwide. Some key outcomes of the current state-of-the-art research have been greater understanding of the air-water flow motion and interactions between turbulence and entrained air, across a relatively broad spectrum of chute slopes (Chanson et al. 2015). Unfortunately, quantitative observations of prototype stepped spillways are too few, because of the great difficulties to successfully perform intrusive measurements. Many unanswered questions remain about the extrapolation of laboratory results to full-scale prototype spillways, typically operating with unit discharges that are 100–1,000 times larger than in the largest laboratory facilities and Reynolds numbers well in excess of 10^6; that is, *how can we trust laboratory results in absence of full-scale validation?*

An unique opportunity for field observations was provided at the Hinze Dam Stage 3 (Gold Coast, Australia). During several major flood events, detailed visual observations were undertaken, showing a number of recurrent features presented herein. The current contribution examines the hydrodynamics of and mechanisms leading to air entrainment in skimming flows on a prototype stepped spillway across a broad range of Reynolds (Re) numbers, $0.68 \times 10^7 < \mathrm{Re} < 10.8 \times 10^7$. In addition to visual observations, the air-water surface flow properties were investigated with some optical flow technique.

Study Site, Methodology, and Flood Events

Located in eastern Australia [Fig. 1(a)], the Hinze Dam was first completed in 1976, and heightened in 1989 and 2011. The (present) Hinze Dam Stage 3 spillway system consists of a compound ogee

[1]Professor in Hydraulic Engineering, School of Civil Engineering, Univ. of Queensland, Brisbane, QLD 4072, Australia. ORCID: https://orcid.org/0000-0002-2016-9650. Email: h.chanson@uq.edu.au

Note. This manuscript was submitted on July 14, 2021; approved on June 12, 2022; published online on September 9, 2022. Discussion period open until February 9, 2023; separate discussions must be submitted for individual papers. This paper is part of the ***Journal of Hydraulic Engineering***, © ASCE, ISSN 0733-9429.

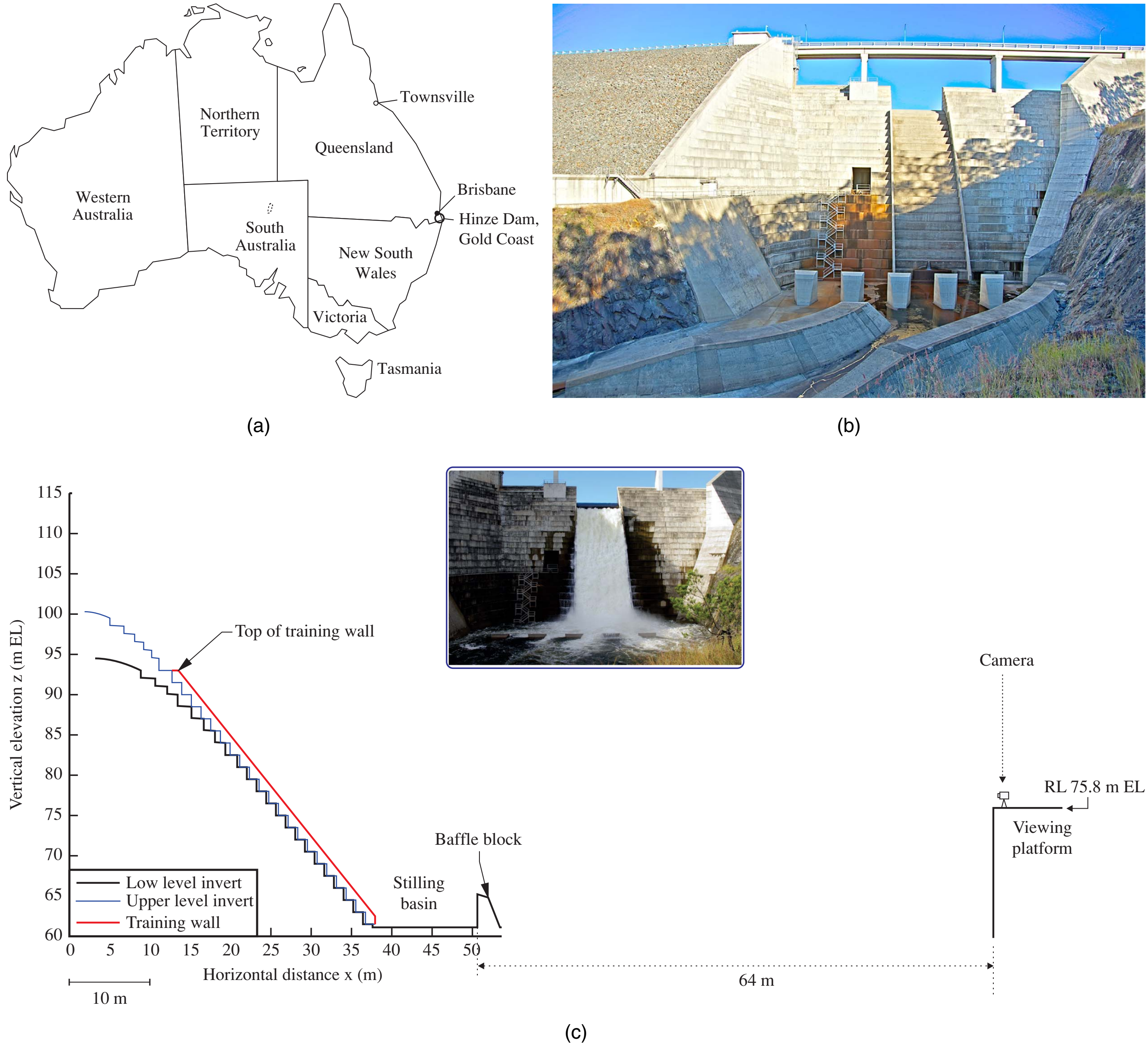

Fig. 1. Hinze Dam Stage 3 spillway (Australia): (a) geographical location of the Hinze Dam, Gold Coast (Australia); (b) photograph of the stepped spillway on June 27, 2014, from the viewing platform facing the stepped chute (the bridge crossing the spillway crest is seen above the crest); and (c) dimensioned undistorted sketch (inset: operation on May 3, 2015, photographed from the viewing platform).

crest followed by a steep stepped chute, ending in a stilling basin with baffle blocks (Phillips and Ridette 2007; SEQWATER 2011a, b, c, d, e, f) [Fig. 1(b)]. The compound ogee crest includes a low level section and two high level sections. The stepped chute has a 1V (vertical):0.8H (horizontal) slope ($\theta = 51.3°$) with 1.5 m high steps ($h = 1.5$ m). Visual observations and video recordings were conducted from two key locations: (1) the bridge above the spillway crest, with the cameras located above the low level section centerline; and (2) a viewing platform facing the stepped spillway [Figs. 1(b and c)].

The overflow discharge was calculated based upon the measured reservoir elevations for the United States Bureau of Reclamation (USBR) ogee crest design (USBR 1965; Chanson 2004). The photographic and video observations were undertaken with digital single lens reflex (dSLR) cameras [Pentax K-01 (Ricoh, Japan), Pentax K-7 (Ricoh, Japan), Pentax K-3 (Ricoh, Japan)] equipped with prime lenses, which produced images with negligible degree of barrel distortion, and a digital camera Casio Exilim EX-10 (Casio, Japan). Further details of the camera sensor resolution and lens characteristics were given by Chanson (2021).

Data Processing

A number of seminal air-water surface features were analyzed in the inception region. The pseudorandomness of occurrence, optical quality and lighting conditions (e.g., under heavy rainfall conditions), and broad range of air-water surface shapes constituted a massive challenge for some automated pattern recognition. Thus, the tracking and measurements of the air-water surface features were conducted manually to guarantee a sound reliability and the best

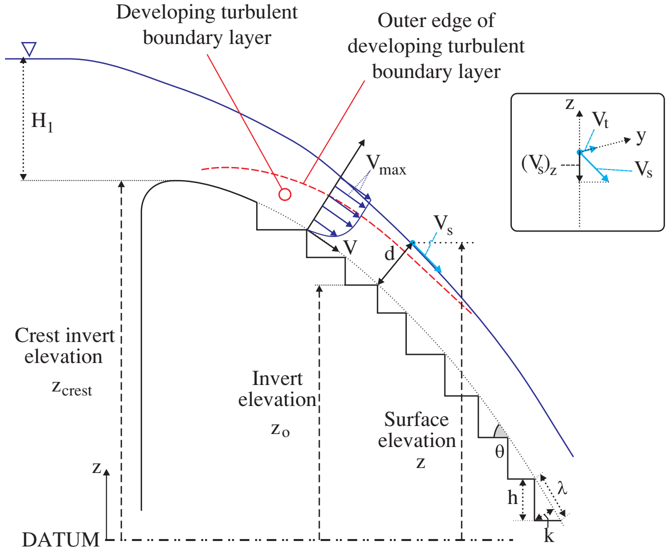

Fig. 2. Definition sketch of the surface velocity components V_s and OF data.

quality control. Their geometrical characteristics (e.g., widths and growth rates) were identified from video movies for the surface scars and from high-shutter speed photographs for the transient elongated air-water surface features. The image analyses of surface scars considered single entities, up to and prior to any collapsing or merging with another feature. The focus of the movie analyses was on the transient properties, such as the surface scar production rate, final transverse dimension, life span, and transverse growth rate, based upon recordings from the bridge overlooking the spillway crest. The elongated air-water surface features in the vicinity of the inception region were best documented with high-shutter speed photography, with an exposure time less than 1 ms, taken from the viewing platform located downstream of the stilling basin. While the use of photographs reduced the amount of available data, the high spatial and temporal resolution of the images enabled a detailed fine geometrical characterization.

Optical flow (OF) is a set of tools, detecting the flow motion between consecutive frames, based upon the brightness constancy assumption (Horn and Schunck 1981). Although originally developed for computer vision, the OF technique may be applied to fluid flows including self-aerated flows (Liu and Shen 2008; Bung and Valero 2016; Zhang and Chanson 2018). In the current study, the Farneback OF technique was used to compute the instantaneous surface velocity field, following Arosquipa Nina et al. (2021) because of its robustness and relative simplicity. The OF was applied to movies taken from cameras installed on a sturdy tripod located on the viewing platform. Detailed postconstruction plans (SEQWATER 2011a, b, c, d, e, f) provided the necessary field data, especially the ground reference points, using landmarks and cross-sectional transects. The positioning of the ground reference points in the spillway and in the image was precisely done. Standard uncertainties of 10 mm and 2–5 pixels were assumed for the ground reference point coordinates and image coordinates, respectively. The corresponding physical resolutions of the videos ranged between 0.01 and 0.12 m per pixel in both horizontal and vertical directions.

The OF surface velocity V_s was systematically compared to the ideal fluid flow velocity V_{max} derived from the application of the continuity and Bernoulli principles

$$\mathrm{V_{max}} = \sqrt{2 \times \mathrm{g} \times (\mathrm{H_1} + (\mathrm{z_{crest}} - \mathrm{z_o}) - \mathrm{d} \times \cos\theta)} \tag{1}$$

where g = gravity acceleration; H_1 = upstream head above the spillway crest; z_{crest} = spillway crest elevation; z_o = invert elevation corresponding to the surface observation location; and d = water depth measured normal to the pseudoinvert formed by the step edges (Fig. 2). Eq. (1) assumes implicitly a hydrostatic pressure and neglects air entrainment and total drag losses. Typical comparisons are presented in Fig. 3, showing the streamwise surface

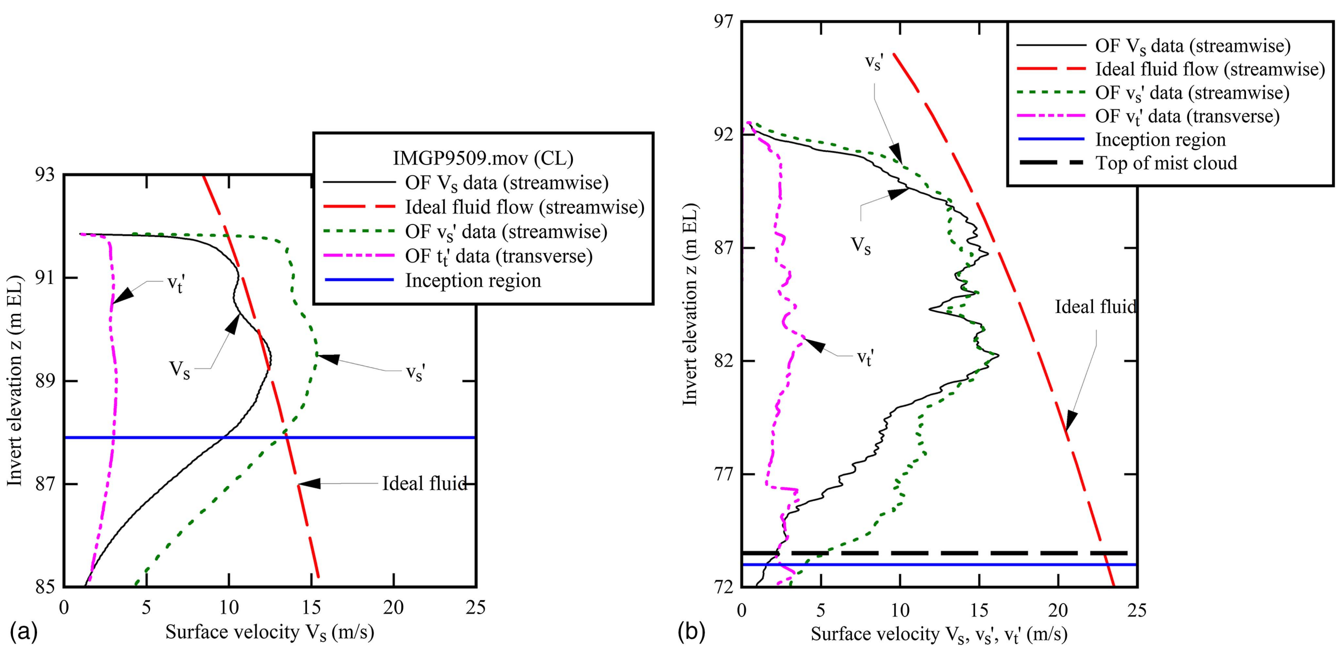

Fig. 3. OF surface velocity at the Hinze Dam stepped spillway, comparison between OF surface velocity data and ideal fluid flow velocity: (a) on March 24, 2021, $Q = 140\ \mathrm{m^3/s}$, $d_c/h = 1.58$, $\mathrm{Re} = 4.5 \times 10^7$, movie resolution: 0.0105 m/pixel (px); and (b) on March 31, 2017, $Q = 334\ \mathrm{m^3/s}$, $d_c/h = 2.82$, $\mathrm{Re} = 10.8 \times 10^7$, movie resolution: 0.035 m/px.

Table 1. Prototype flow conditions for observations at the Hinze Dam Stage 3 stepped spillway operation (low level section)

θ (°)	h (m)	Date	H_1[a] (m)	Q (m^3/s)	q (m^2/s)	d_c/h	Re	Comment
51.3	1.5	01/29/2013	4.2	202	16.5	2.02	6.5×10^7	See also Chanson (2013)
		05/3/2015	0.98	20.9	1.71	0.44	0.68×10^7	
		03/31/2017	5.76	334	27.3	2.82	10.8×10^7	1:100 year flood event
		03/23/2021	2.88	111	9.05	1.35	3.6×10^7	
		03/24/2021	3.34	140	11.4	1.58	4.5×10^7	
		03/27/2021	2.18	71.7	5.86	1.01	2.3×10^7	

Note: d_c = critical flow depth; h = vertical step height measured from step edge and step edge; Q = water discharge; q = unit discharge; Re = Reynolds number defined in terms of the hydraulic diameter; and θ = slope between pseudobottom formed by step edges and horizontal.
[a]Data from Bureau of Meteorology (BOM) (Station Number: 040847, Name: Nerang R at Hinze Dam #, Owner: SEQwater:146906).

velocity component V_s as a function of the vertical elevation z of the free surface. In each graph, the solid horizontal line is the average location of the inception of free-surface aeration, and the dashed horizontal line in Fig. 3(b) is the position of the top of the mist cloud above the stilling basin. The ideal fluid flow estimate are plotted in thick dash line in Fig. 3. Overall the data showed a relatively close agreement between the longitudinal OF surface velocity and the ideal fluid flow velocity upstream of the inception region, both qualitatively and quantitatively. In contrast, the agreement was very poor in the air-water flow region downstream of the inception region of free-surface aeration.

Discussion on Optical Flow Data Quality, Noise, and Errors

With surface flow movies, the OF data quality was diversely affected by several issues, although the optical artifacts were very different from laboratory observations (Zhang and Chanson 2018; Arosquipa Nina et al. 2022). The images included the upstream nonaerated free surface, the inception point region, and self-aerated free-surface downstream of the inception region, as well as the upper level sections on both sides and sometimes the stilling basin. The flow region upstream of the inception location and the inception region generated fewer artifacts in the surface flow, in contrast to the experience of Arosquipa Nina et al. (2022) with top view movies in laboratory. The Hinze Dam overflow was opaque and dark brown, evidence of sediment suspension and organic matter transport, contrasting vividly with the clear-water quasi-translucid waters in laboratory studies. Herein, the self-aerated flow region yielded inaccurate surface velocity data because of the limited video movie frame rate and the very bright white waters. The adjustment of the brightness of the white waters was most challenging and near impossible in the field conditions. The limited frame rate of the cameras was too slow to characterize completely the turbulence characteristics, in the author's opinion. At the downstream end of the chute, the plunge point was highly fluctuating, inducing substantial optical noise in the form of surface waves above the baffle blocks and mist plume rising above the plunge point and stilling basin.

Practically, the quality of the OF data was closely linked to the quality of the original movies, including (1) location of the camera, with better quality for movies perpendicularly facing the spillway chute, although sometimes impossible owing to wind conditions and mist depositing on the camera lens, (2) quality of the photographic equipment (i.e., camera and lens), with the better image quality obtained with professional-grade (expensive) prime lenses, (3) movie resolution, with better outputs with better resolutions and smaller meter per pixel, (4) light conditions (e.g., with very poor outputs in heavy rain conditions), and (5) experience of the operator, with gradually better movie image quality from 2013, 2015, to 2017–2021.

Finally, it must be stressed that the present OF image processing used a simple and robust method, the Farneback technique, applying a set of parameters previously validated in laboratory by Arosquipa Nina et al. (2021). No attempt was made to calibrate the OF calculations.

Flood Events

The prototype observations were conducted for water discharges between 20.9 and 334 m^3/s, corresponding to dimensionless discharges d_c/h between 0.44 and 2.82, and Reynolds numbers between 6.8×10^6 and 1.08×10^8, with d_c the critical flow depth and h the step height (Table 1). Table 1 lists the details of the experimental flow condition. For all field observations, the overflow discharge was contained in the low level section of the spillway ($B = 12.25$ m).

Some key novel features of the present data set were a series of observations (1) by the same individual with extensive expertise in stepped spillway hydraulics, (2) using similar photographic equipment of high quality and same photographer, (3) at a facility with excellent optical/visual access, and (4) ease of physical access to bring the equipment. As with any field measurements, there were a number of uncontrolled parameters, including the lighting conditions, mist and spray advected over the stilling basin, and dropping on the camera lenses. For example, some thick mist above the stilling basin adversely affected the image quality and OF results at the downstream end of the chute.

Flow Patterns

The visual observations showed a number of recurrent features during all the flood events. Upstream of the inception region, the free surface presented some undular wavy surface pattern, in phase with the stepped invert profile. Immediately upstream of the inception region, large-scale turbulent structures were seen to interfere with the free surface, in the form of large well-marked scars and boils, first highlighted by Chanson (2013) (Fig. 4). Fig. 4 presents several examples of turbulence-surface interactions. Note the different shutter speeds between Figs. 4(a–c), owing to the different light conditions. The free-surface aeration was caused by the very strong turbulence acting next to the free surface in the water phase (Ervine and Falvey 1987; Brocchini and Peregrine 2001; Chanson 2009). In terms of the source of vorticity, Levi (1965) argued the development of longitudinal vortices during the rapid flow acceleration at the spillway crest, while Toro et al. (2017) hinted that the vortical structures were issued from the first step edge and stepped cavity, with more recent computational fluid dynamics (CFD) results showing the instantaneous deformation of the free surface as a result of vortical structure interactions (Zabaleta and Bombardelli 2020). At the Hinze Dam stepped spillway, the surface scars

J. Hydraul. Eng., 2022, 148(11): 05022004

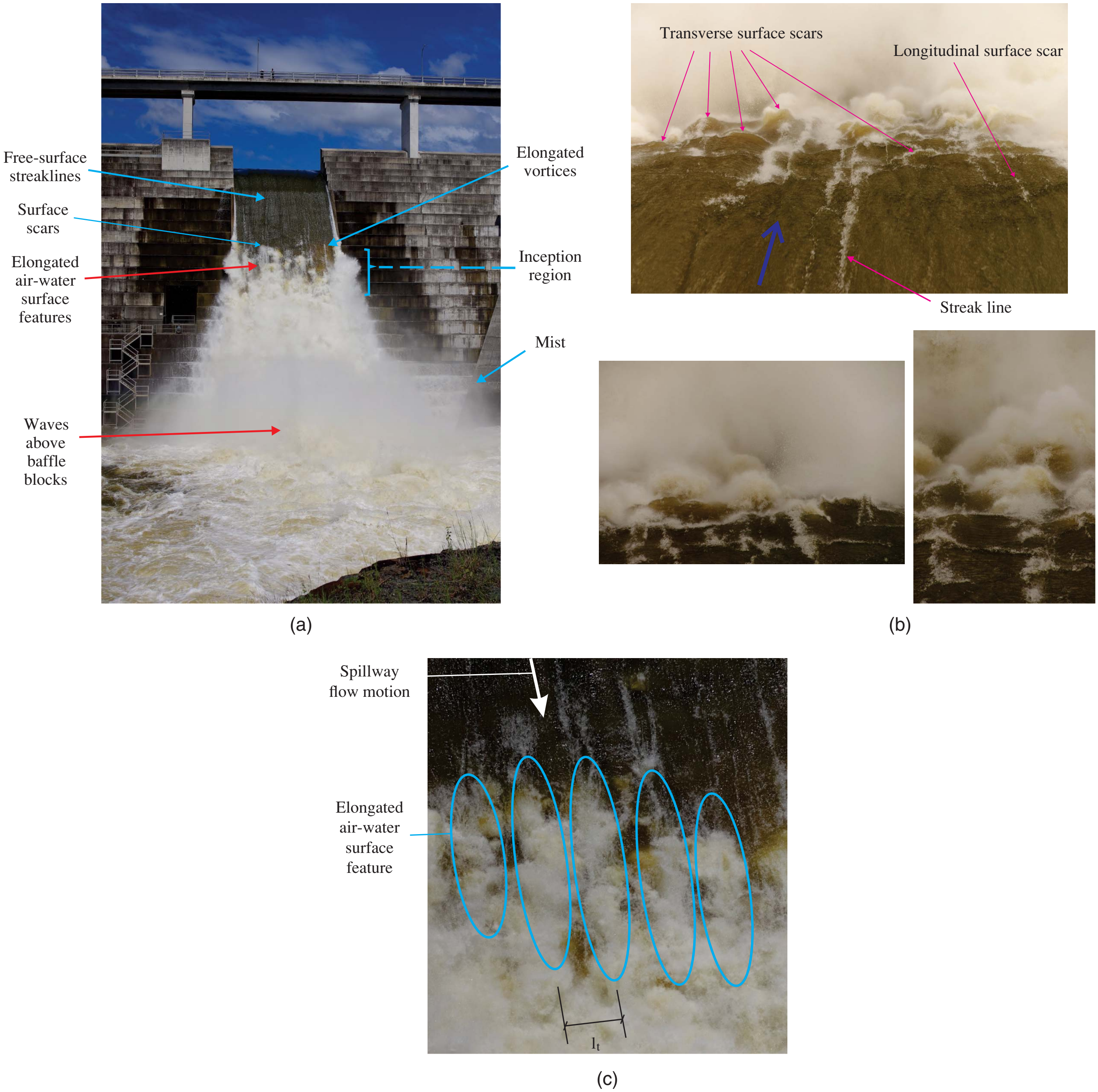

Fig. 4. Air-water surface features during the stepped spillway operations at the Hinze Dam Stage 3: (a) self-aerated free-surface flow on Hinze Dam Stage 3 stepped spillway on March 24, 2021, $Q = 140\ \mathrm{m^3/s}$, $q = 11.4\ \mathrm{m^2/s}$, $d_c/h = 1.58$, $\mathrm{Re} = 4.5 \times 10^7$ (shutter speed: 1/2,500 s); (b) interactions between large-scale turbulent structures and water surface in the vicinity of the inception at Hinze Dam stepped spillway on March 31, 2017, for $Q = 334\ \mathrm{m^3/s}$, $q = 27.3\ \mathrm{m^2/s}$, $d_c/h = 2.82$, $\mathrm{Re} = 10.8 \times 10^7$, views from above the spillway crest looking downstream (shutter speed about 1/200 s); and (c) elongated air-water surface features in the vicinity of the inception region on March 24, 2021, for $Q = 140\ \mathrm{m^3/s}$, $q = 11.4\ \mathrm{m^2/s}$, $d_c/h = 1.58$, $\mathrm{Re} = 4.54 \times 10^7$ (shutter speed: 1/8,000 s).

highlighted the interaction of one or more tilted quasi-streamwise vortices with the water surface (Fig. 5). The interactions and collisions of these structures with the free surface could be explosive, with air-water packets surging upward through the free surface and extreme eruption events reaching in excess of 1 m above the water surface, immediately downstream of the inception region.

The position of the onset of free-surface aeration was constantly fluctuating about a mean location (Fig. 4). At a given instant, the inception point was not a straight line, but rather a surface plane with some transient pattern, called herein the inception region. A similar pattern and elongated air-water surface features were also observed in the inception region of the Paradise Dam (Biggenden,

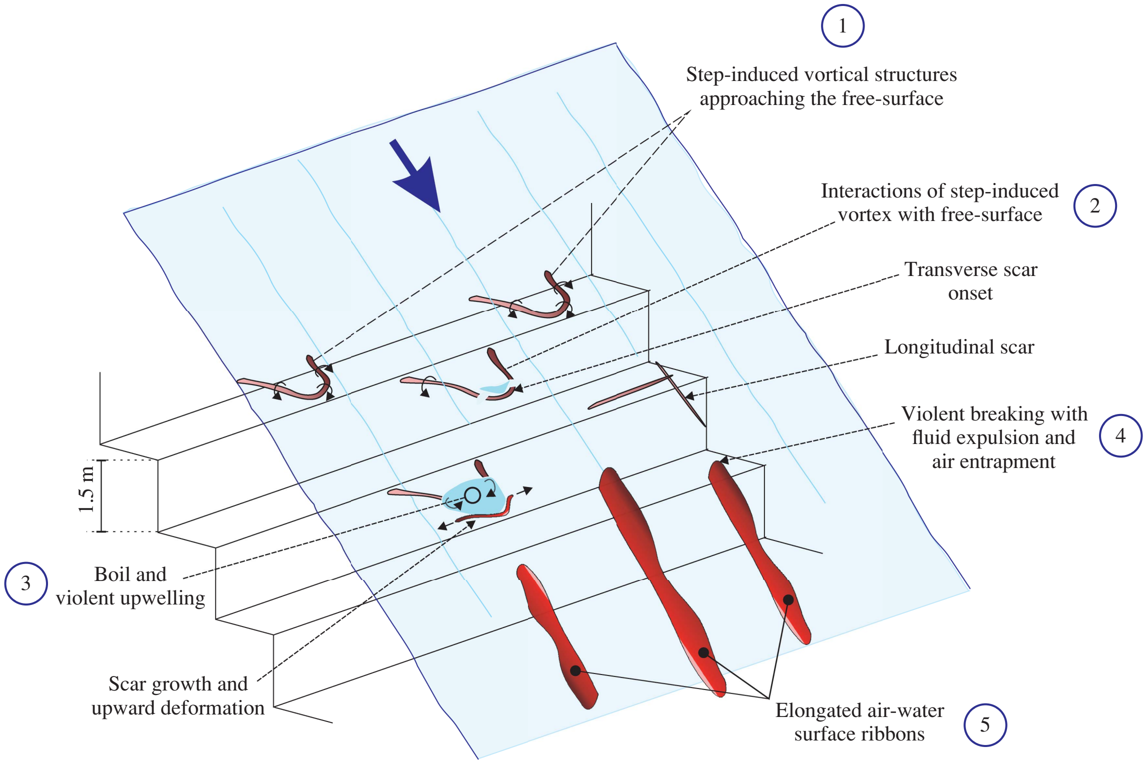

Fig. 5. Interactions between step-induced turbulent structures and free surface at the inception region in skimming flow above a stepped spillway.

Queensland, Australia) stepped spillway on March 5, 2013 by the author. High-shutter speed photographs showed the presence of short-lived elongated air-water surface features [Figs. 4(a and c)], somehow similar to those shown by Levi (1965) at Miguel Hidalgo Dam spillway (El Fuerte, Mexico), observed at the Paradise Dam stepped spillway by the author, and discussed by Arosquipa Nina et al. (2021) in a large-size stepped spillway model. These elongated air-water surface features in the vicinity of the inception region were best documented with high-shutter speed photography (see "Elongated Air-Water Surface Features in Skimming Flows" section below).

Downstream of the inception region, the spillway overflow was white, with some complicated mix of air and water with an intricate inner structure (Chanson 1997; Brocchini 2002). The upper free surface was further the locus of air-water surface waves, illustrated at Chinchilla Weir (Chinchilla, Queensland, Australia) and Three Gorges project (Yichang, China) (Toombes and Chanson 2007). At the downstream end of the stepped spillway, the high-velocity air-water flow impinged into the stilling basin in a plunging jet motion, for the observed flood flow conditions. A strong mist was generated at the impingement, rising upward above the stilling basin [Fig. 4(a)]. The thick mist could raise more than 10 m above the stilling basin water surface, with fine droplets traveling further away and reaching the viewing platform located over 75 m away from the chute toe. Visually, the nature and extent of the mist appeared comparable to the mist generated at Paradise Dam stepped spillway, as observed by the author on March 5, 2013. In the stilling basin, the air-water flow was highly turbulent as the combined result of the impingement of the high-velocity chute flow on the stilling basin invert and on the baffle blocks. The water surface was extremely chaotic above the baffle blocks with air-water waves, reaching instantaneous heights over 6 m in March 2021.

Air-Water Surface Features

Elongated Air-Water Surface Features in Skimming Flows

At high discharges corresponding to a skimming flow regime, the inception region presented a network of transient elongated air-water surface features [Figs. 4(a and c) and 5]. These highly aerated ribbons were much longer than wide, with an aspect ratio in excess of 10. In between these air-water ribbons, clear-water valleys/troughs were observed. The elongated air-water features were believed to play a key role in the inception of free-surface aeration. Their existence might be linked to the well-documented presence of longitudinal coherent structures on the scale of the boundary layer thickness forming at the outer edge of turbulent boundary layers (Robinson 1991). As the boundary layer developed, the three-dimensional bulges interacted with the free surface while the deep irrotational valleys on the edges of the vortices contributed to some fluid entrainment into the turbulent region, including air entrainment once the turbulent kinetic energy would overcome the surface tension (Ervine and Falvey 1987; Chanson 2009). Additionally, Levi (1983) associated the existence of these structures to internal local oscillations within the water column, expanding Roshko's (1954) universal Strouhal law, and he linked their transverse spacing to spanwise standing waves within the boundary shear flow.

The instantaneous numbers of ribbons and troughs were recorded based upon a large number of high-shutter speed photographs. The results are presented in Fig. 6(a), as a series of histograms of the instantaneous number of clear-water valleys/troughs in the near proximity of the inception region. While all the data showed some pseudonormal distribution, the number of clear-water valleys, hence the number of elongated air-water surface features, tended to

J. Hydraul. Eng., 2022, 148(11): 05022004

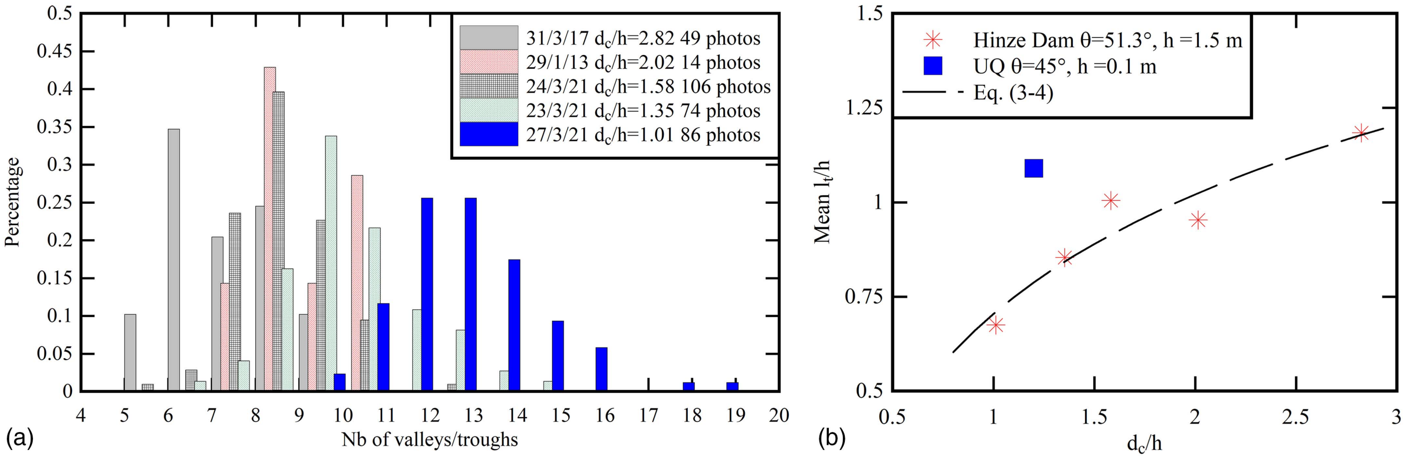

Fig. 6. (a) Histograms of instantaneous number of clear-water valleys/troughs across the low level chute width ($B = 12.25$ m) in the vicinity of inception region on the Hinze Dam stepped spillway, legend gives the number of photographs; and (b) dimensionless average transverse spacing l_t/h of air-water ribbons in the vicinity of the inception region, comparison with laboratory data from Arosquipa Nina et al. (2021) and Eq. (2). UQ = University of Queensland

increase with decreasing flow rate. The trend is illustrated in Fig. 6(a) in a dimensionless form, showing the average transverse spacing l_t between elongated air-water surface features as a function of the dimensionless discharge. The data are further compared to observations in a large-size stepped flume in Fig. 6(b). The results showed an increasing dimensionless transverse spacing l_t/h with increasing dimensionless discharge d_c/h, with a reasonable agreement between prototype and laboratory data despite some difference in scales and conditions. For the Hinze Dam observations, the data were best fitted by

$$\frac{l_t}{h} = 0.705 + 0.456 \times Ln\left(\frac{d_c}{h}\right) \quad \text{for } 0.6 < d_c/h < 2.9 \tag{2}$$

with a normalized correlation coefficient $R = 0.947$. Eq. (2) is compared to the data in Fig. 6(b).

The present observations at Hinze Dam emphasized a three-dimensional inception process, illustrated in the conceptual model presented in the next subsection. The present evidences of air entrapment onset by three-dimensional longitudinal structures demonstrate that the conceptual models based upon two-dimensional chute flow (e.g., Wood et al. 1983, Fig. 1; Chanson 2009; Fig. 3(a); Valero and Bung 2018, Fig. 1) are clearly simplistic.

Surface Scars Upstream of Inception Region in Skimming Flows

In an open channel flow, many complex free-surface structures (e.g., boils) may be induced by a combination of the generation of large-scale vortices by an invert with macroroughness (e.g., dunes and steps) and their upwellings to the free surface (Sarpakaya 1996; Best 2005). In the near proximity below the free surface, the coherent structures are sustained by and have their roots in the three-dimensional turbulence induced by the invert. Yet, any turbulence approaching the water surface may be restructured, becoming quasi-two-dimensional at the free surface, while the merging of same-sign vortices and cancellation of opposing vortices shift the coherent structure size distribution toward larger scale (Galanti and Sulem 1991). In the presence of very strong turbulence like on a stepped spillway, the fluctuating eddies are no longer restrained by the inertia and surface tension, once they interact with the free surface, and the water surface may explode when water blobs approaching the surface maintain their speed and are ejected. At the same time, the ejected fluid is replaced by entrapped air, leading to an emulsion of air and water. Although the topic has been previously discussed in a wider range of applications (Hino 1961; Ervine 1998; Lubin and Chanson 2017), our current knowledge of these extremely complicated air-water flows remains limited (Wood 1991; Chanson et al. 2021). At the Hinze Dam stepped spillway, some transient surface scars were observed immediately upstream of the inception region [Fig. 4(b)]. The surface scars tended to develop primarily as transverse entities, although both longitudinal and transverse scars were observed. The visual observations suggested a common topology of macroturbulence-free-surface interactions in stepped chute skimming flow, consisting of some pseudohairpin tubular vortex head that, when interacting with the free surface, provides a strong deformation and ultimately some breaking of the surface. The observations across several major flood events allowed the proposition of a conceptual model to explain the patterns of upwelling and inception of free-surface aeration in skimming flows (Fig. 5).

The onset of free-surface aeration tended to follow five stages, sketched in Fig. 5. First, large step-induced tilted vortical structures, approaching the free surface, started to deform the water surface. The very-large-scale coherent structures were shed into the outer flow, likely assisted by flapping of the shear layer developing downstream of each step edge, with a possible contribution from free-surface instabilities. The large vortices presented a tilted tubular pseudohairpin shape similar to the conceptual sketched proposed by Theodorsen (1952) (Figs. 1 and 3), likely convected within some complicated three-dimensional network structure as the coherent structures developed in the outer flow (e.g., Imamoto and Ishigaki 1986; Toro et al. 2017).

Second, the vortex head attached to the free surface when it encountered the interface, generating a mostly transverse scar, while the neck interacted with the free surface. Third, some violent upwelling took place when the legs of the vortex interacted with water surface in the wake of the scar. This stage was often characterized by a very rapid growth of the scar. As the eruption developed, some upward stretching of the scar occurred, with violent breaking, air-water fluid expulsion and air entrapment (fourth stage). While the upwelling continued, the eruption and surface breaking led to the formation of elongated air-water surface

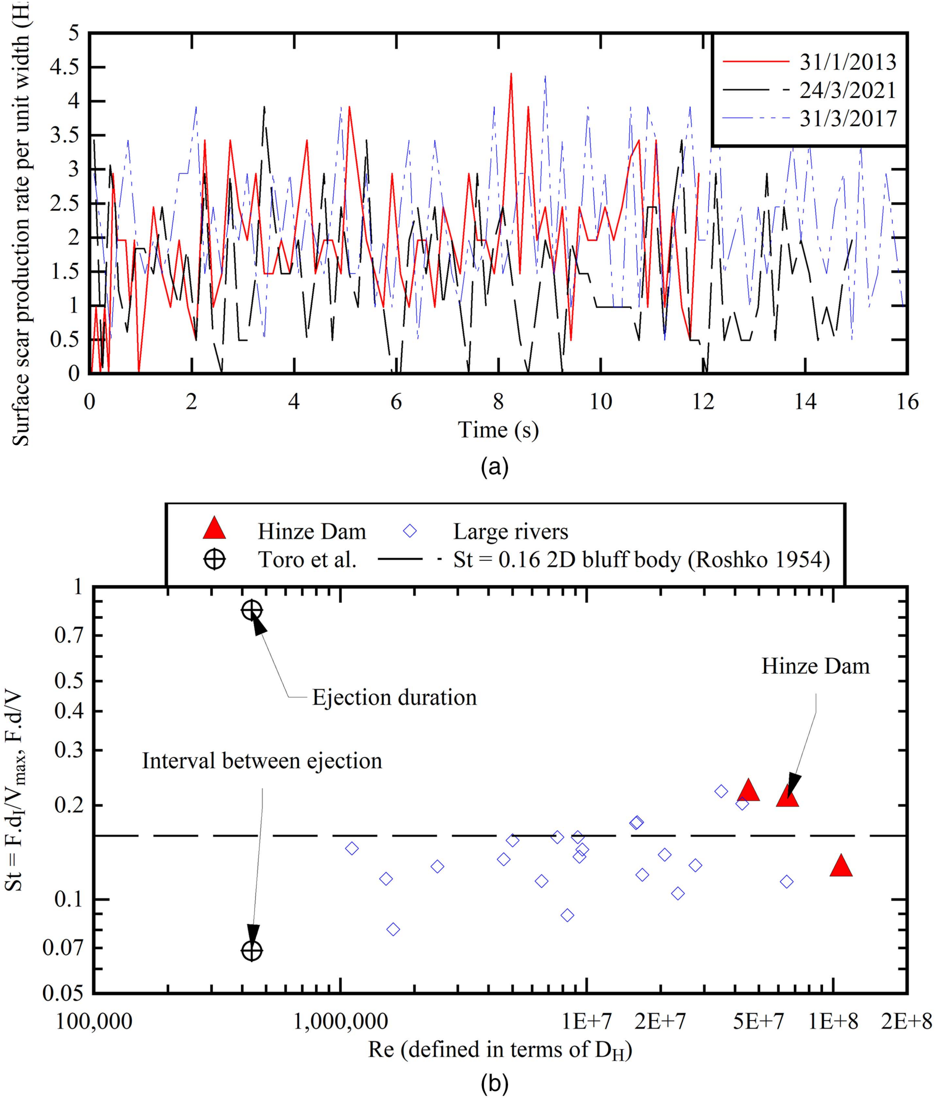

Fig. 7. Generation of surface scars and frequency of surface scar generation rate immediately upstream of the inception region of free-surface aeration on the Hinze Dam stepped spillway: (a) time-variation of production rate of surface scars per unit width; and (b) scaling of mean frequency of surface scar generation rate fluctuation: Strouhal number versus Reynolds number, comparison with cavity ejection frequency with stepped spillway (data from Toro et al. 2017), surface boils in large rivers with dune bed forms (data from Korchokha 1968; Jackson 1975; Barua and Rahman 1998) and Roshko Strouhal law (data from Roshko 1954; Levi 1983).

ribbons (fifth stage) (Fig. 5). The growth of the elongated air-water surface features would then lead to the complete aeration of the whole free surface (i.e., the white water region downstream of the inception region). The five stages are highlighted in Fig. 5.

This general pattern of inception motion could be observed at the water surface for all discharges (Table 1), and extended previous limited visual observations of skimming flows on stepped spillway (e.g., by the author at Hinze Dam, Paradise Dam, and Gold Creek Dam, and by Professor Jorge Matos at Pedrogao Dam). Altogether, the onset of aeration was a highly transient process, starting with the generation of surface scars and followed by some violent upwelling and breaking associated with a combination of energetic explosions and implosions of the water surface that could not be contained by neither surface tension nor gravity. The whole process was unsteady and three-dimensional.

The visual data showed a large generation rate of surface scars. Typical quantitative data are shown in Fig. 7(a), with the production rate per unit width as a function of time. Herein, a scar generation was defined as the onset of the scar development [i.e., the smallest surface disturbance at the initiation of the scar (Fig. 5, Stages 1 and 2)]. The time history of individual scars suggested three development stages; that is, (1) an initially slow growth, then (2) a very rapid transverse growth with transverse growth rate well in excess of 10 m/s, lasting 0.015–0.025 s, often associated with some light spray and splashing, and later (3) a slower transverse growth combined with an upward deformation of the scar structure (Fig. 5, Stage 3), until the scar collapsed, exploded, imploded, merged, or disappeared. During the initial growth, the scar length increased with time from $t^{0.4}$ to $t^{0.8}$, while the scar growth rate followed from about $t^{2.4}$ to $t^{3.7}$ during the second phase characterized by the rapid growth in transverse scar dimension. This marked change in growth rate between the first two phases was clearly observed qualitatively and quantitatively (Chanson 2021). The time variations of the scar generation rate presented large fluctuations [Fig. 7(a)]. The data showed some characteristic periodicity of scar appearance at a point on the water surface, with mean periods between 0.4 and 0.5 s.

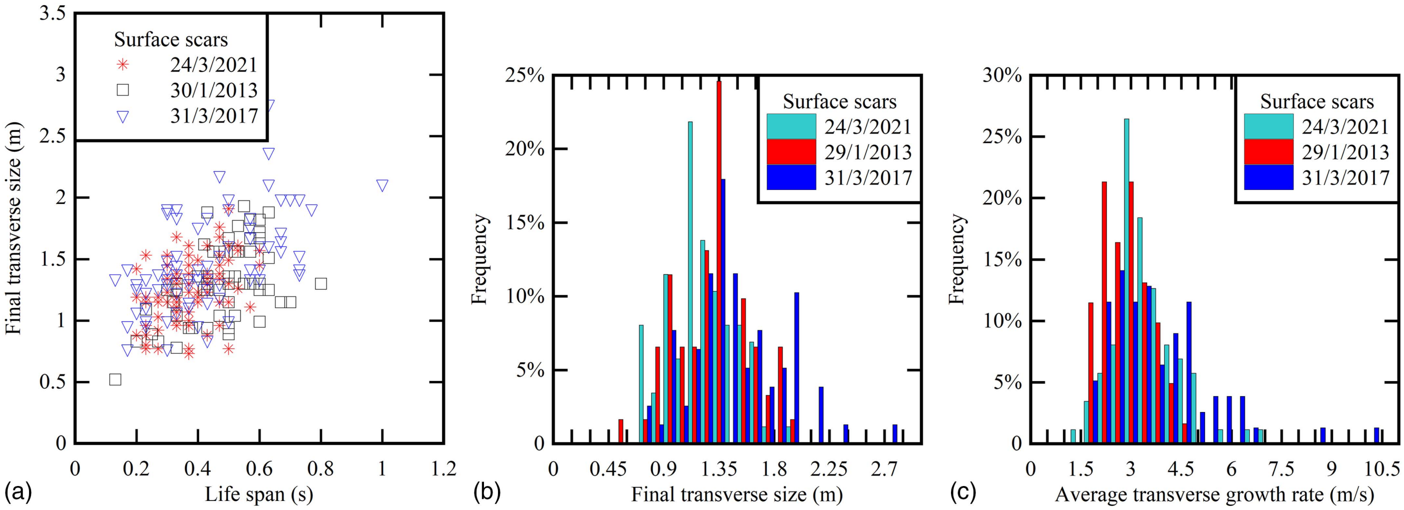

Fig. 8. Individual surface scar characteristics immediately upstream of the inception region of free-surface aeration: (a) final transverse size as a function of the lifespan between first appearance and disappearance; (b) final transverse size; and (c) average transverse growth rate between first appearance and disappearance.

The data are reported in a dimensionless form in Fig. 7(b), where F is the characteristic frequency in scar generation rate fluctuations. Herein, the Strouhal number is defined in terms of the water depth and surface velocity in the inception region: $St = F \times d_I / V_{\max}$, with $V_{\max}$ the ideal fluid free-stream velocity and d_I measured based upon the water level on the training walls. In Fig. 7(b), the present data (triangles) are compared to the surface boil frequency data in large rivers, and ejection frequency data on stepped spillway. The latter data set is based upon the CFD computations of Toro et al. (2017) in the developing flow region of a laboratory stepped chute, and the data are presented in terms of the cavity ejection duration (upper point) and interval between cavity ejection (lower point), immediately upstream of the inception region [Fig. 7(b)]. Overall, the fluctuations in surface scar generation rate were believed to be linked to the time interval between successive stepped cavity ejections.

The growth of individual scars was recorded from onset to disappearance. Fig. 8(a) presents the final transverse size of surface scars as a function of their lifespan. Although the data were scattered, the trend indicated overall an increased size with increasing lifespan. The present observations showed that the surface scars developed initially as transverse structures primarily for $d_c/h = 1.58$ and 2.02. In contrast, the observations for the largest discharge $d_c/h = 2.82$ indicated the development of a number of longitudinal scars, in quantities almost as large as transverse scars. The final transverse size was between 1.2 and 1.5 m in average, with an average final size increasing with overflow discharge [Fig. 8(b)]. The average scar growth rate was about 3–4 m/s, between inception to disappearance [Fig. 8(c)]. However, much larger transverse growth rates were reported during the rapid growth sequence (Stages 2 and 3, Fig. 5), with instantaneous growth rates of up to 25 m/s.

Inception of Free-Surface Aeration

At the upstream end of the steep stepped chute, a bottom turbulent boundary layer was generated by the total drag on the invert and developed through the water column, with an increasing boundary layer thickness with increasing distance from the spillway crest (Amador et al. 2006; Bombardelli et al. 2011; Zhang and Chanson 2016a, b) (Fig. 2). Once the turbulence next to the outer edge of the turbulent boundary layer interacted with the overflow water surface, a strong free-surface aeration took place, as proposed by Lane (1939) and others (Halbronn 1952; Wood et al. 1983). On both smooth and steep stepped chutes, the experimental observations suggested that the inception conditions were achieved when the boundary layer thickness reached about 80% of the water depth (Wood 1985; Zhang and Chanson 2016a). Note that the aforementioned conceptual model is relevant to steep spillways, but not flat-slope chutes, in which self-aeration may occur in partially developed flow as a result of the development of free-surface instabilities, upstream disturbances, and longitudinal vortices (Levi 1965; Anwar 1994).

At the Hinze Dam stepped spillway, the *inception point* of free-surface aeration was a surface plane characterized by very strong interactions between the flow turbulence and free surface. Visual, photographic, and cinematographic observations suggested that the instantaneous location of the inception region varied with both time and transversal location. Altogether, the inception region was encompassed about the mean inception region location L_I, shown in Fig. 3 and reported in Fig. 9, plus and minus two step cavities, with L_I the distance between the spillway crest and the time-averaged position of inception region. For all prototype observations, the mean location of the inception region was recorded visually, as well as the flow depth at that location. The dimensionless location of the inception region is shown in Fig. 9(a), presenting the dimensionless location L_I/h as a function of the dimensionless discharge d_c/h. With increasing overflow discharge Q, the onset of free-surface aeration occurred further downstream on the stepped slope. The finding was consistent with some detailed observations on a 45° (1V:1H) stepped laboratory chute (Zhang 2017; Zhang and Chanson 2018; Arosquipa Nina et al. 2021), although the present data tended to be slightly more upstream than other prototype data (Table 2) for the same dimensionless discharge [Fig. 9(a)].

In Fig. 9(a), the dimensionless location of the inception region is compared to some analytical expression based upon some turbulent boundary layer growth model (Chanson 1994)

$$\frac{L_I}{h} = 9.719 \times (\sin\theta)^{0.0796} \times \cos\theta \times F_*^{0.713} \quad (3)$$

where θ = chute slope (i.e., $\theta = 51.3°$) for the Hinze Dam Stage 3 stepped spillway; and F_* = dimensionless Froude number defined

J. Hydraul. Eng., 2022, 148(11): 05022004

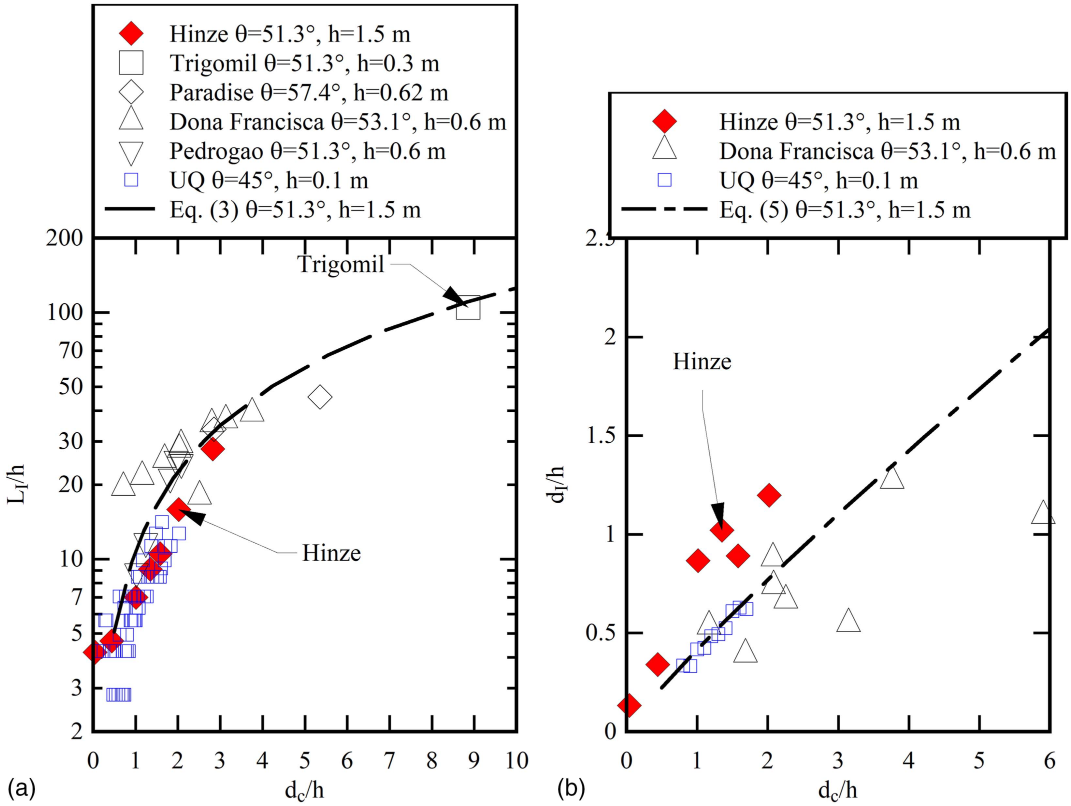

Fig. 9. Characteristic of the inception region at the Hinze Dam Stage 3 stepped spillway, comparison with laboratory observations on a 45° stepped chute (data from Zhang and Chanson 2016a; Zhang 2017; Arosquipa Nina et al. 2021) and prototype observations (Table 2). Both prototype and laboratory data were based upon visual observations: (a) location of the inception region of free-surface aeration, comparison with Eq. (3); and (b) flow depth at the inception region of free-surface aeration, comparison with Eq. (5).

Table 2. Characteristics of and observation flow conditions on prototype steep stepped spillway

Dam	Country	θ (°)	H (m)	B (m)	Study period	Q (m^3/s)	d_c/h	Re	Comment
Hinze	Australia	51.3	1.5	12.25	2013–2021	21–334	0.44–2.82	6.8×10^6–1.1×10^8	Stage 3 low level section
Paradise	Australia	57.4	0.62	335	2010–2013	2,462–6,344	2.85–5.35	2.9×10^7–7.2×10^7	
Trigomil	Mexico	51.3	0.3	75	1992	1,017	8.85	5.4×10^7	During construction
Dona Francisca[a]	Brazil	53.1	0.6	N/A	2007–2009	N/A	0.71–5.91	3.5×10^6–8.3×10^7	
Pedrogao[a]	Portugal	51.3	0.6	301	2010	433–1,258	1.02–2.08	6.0×10^6–1.7×10^7	

Note: B = chute width; d_c = critical flow depth; h = vertical step height measured from step edge and step edge; Q = water discharge; q = unit discharge; Re = Reynolds number defined in terms of the hydraulic diameter; and θ = slope between pseudobottom formed by step edges and horizontal.
[a]Data provided by Professor Jorge Matos.

in terms of the gravity component in the flow direction and step cavity depth

$$F_* = \frac{1}{\sqrt{\sin\theta \times (\cos\theta)^3}} \times \left(\frac{d_c}{h}\right)^{3/2} \tag{4}$$

Eq. (3) is plotted in Fig. 9(a) for $\theta = 51.3°$ and $h = 1.5$ m, showing a good agreement between most data and Eq. (3). The water depth d_I at the inception of free-surface aeration was further recorded and the data are presented in Fig. 9(b) as the dimensionless depth d_I/h being a function of the dimensionless discharged d_c/h. The data showed an increase in flow depth at inception with increasing discharge, despite some scatter. In Fig. 9(b), the data are further compared to some theoretical reasoning yielding an expression of the flow depth at inception (Chanson 1994)

$$\frac{d_I}{h} = 0.4034 \times \frac{F_*^{0.592}}{(\sin\theta)^{0.04}} \times \cos\theta \tag{5}$$

Importantly, the observations at the Hinze Dam Stage 3 spillway were accurate, owing to the excellent physical and optical access, enabling accurate observations with minimum distortion and parallax errors. Thus, the good agreement between some laboratory observations under controlled conditions and the Hinze Dam spillway data tended to validate the quality and accuracy of the present prototype data set.

Surface Velocities

In prototype spillways, velocity measurements are extremely difficult and potentially dangerous if not properly planned, thus rare. Despite new optical technique development in laboratory, the

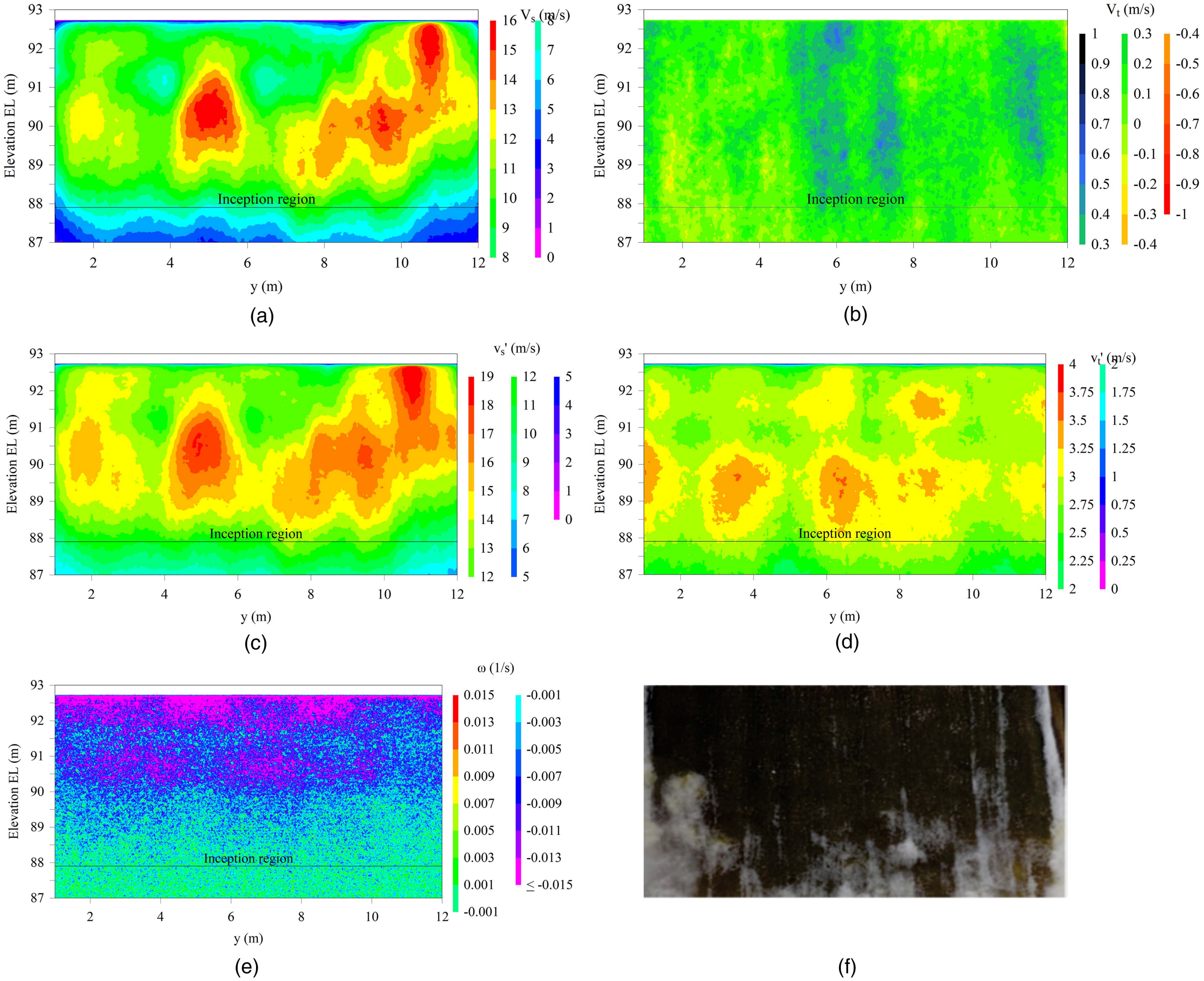

Fig. 10. OF surface velocity data at the Hinze Dam Stage 3 stepped spillway on March 24, 2021, $Q = 140\ \mathrm{m^3/s}$, $d_c/h = 1.58$, $\mathrm{Re} = 4.5 \times 10^7$, movie H2 (resolution: 0.0105 m/px): (a) time-averaged streamwise surface velocity V_s; (b) time-averaged transverse surface velocity V_t; (c) standard deviation of streamwise surface velocity v_s'; (d) standard deviation of transverse surface velocity v_t'; (e) OF surface vorticity data; and (f) field of view.

application to full-scale structures has not been successfully conducted in high-velocity hypercritical flows. The present OF data characterized the longitudinal/streamwise and transverse/spanwise motion of the upper surface of the spillway flow. As discussed previously, the results in the aerated flow region were not reliable. Typical centerline OF surface velocity data are shown in Fig. 3, in terms of streamwise surface velocity component V_s, the streamwise surface velocity standard deviation v_s', and the transverse surface velocity standard deviation v_t'. In Fig. 3, the vertical axis is the vertical elevation z defined in Fig. 1(c) and the horizontal axis is the surface velocity data. Overall, the streamwise surface velocity data showed a relatively close agreement with the ideal fluid flow velocity in the nonaerated flow region, with increasing surface velocity with decreasing vertical elevation as predicted by the Bernoulli principle, although it is acknowledged that the OF data started to deviate from the ideal fluid flow velocity at some distance upstream of the inception region (IR) because of the fluctuating nature of the inception region of free-surface aeration. Large streamwise surface velocity fluctuations were observed for all discharges, while the transverse surface velocity fluctuations were much smaller.

The OF velocity field was analyzed for three flood events, corresponding to dimensionless discharges $d_c/h = 1.0$, 1.6, and 2.8. A typical data set is presented in Fig. 10, in terms of the streamwise and transverse surface velocities (i.e., V_s and V_t, respectively), their standard deviation, and the optical surface vorticity ω defined as

$$\omega = \frac{\partial V_t}{\partial s} - \frac{\partial V_s}{\partial y} \tag{6}$$

In each graph, the vertical axis is the vertical elevation z defined in Fig. 1(c), the horizontal axis is the transverse coordinate y with $y = 0$ at the right training wall, and the legend applies to the OF data. The mean location of the inception region of free-surface aeration is shown as a thick solid line. Finally, Fig. 10(f) illustrates the field of view of the movie. The contour map results confirmed that the OF surface data were physically meaningless downstream of

J. Hydraul. Eng., 2022, 148(11): 05022004

the inception region of free-surface aeration. The OF surface velocity data further suggested the presence of elongated patterns, or streets of surface vortices, with streaks of faster flowing fluid in between. While the position of these surface vortices varied with time, their lateral spacing tended to be well defined, increasing with increasing discharge and water depth [Fig. 6(b)]. These elongated patterns are seen in the contour maps of time-averaged surface velocity and their standard deviation (Fig. 10).

Upstream of the inception region, the surface velocity data showed the acceleration of the flow, with a trend consistent with the ideal fluid flow theory (Keller and Rastogi 1975; Wood et al. 1983). All the data showed large standard deviations of the streamwise surface velocity v_s'. In the proximity of and upstream of the inception region, the dimensionless streamwise fluctuations Tu_s was about unity

$$Tu_s = \frac{\sqrt{\overline{v_s'^2}}}{\overline{V_s}} \approx 1 \tag{7}$$

where $\overline{V_s}$ = time-averaged streamwise velocity being averaged across the chute width; and $\sqrt{\overline{v_s'^2}}$ = standard deviation of the streamwise velocity fluctuations averaged across the chute. The large surface fluctuations were caused by a combination of free-surface turbulence and free-surface fluctuations in the direction normal to the invert. The findings were somehow consistent with laboratory observations of large free-surface fluctuations upstream of the inception region in skimming flows (Chamani 2000; Felder and Chanson 2014; Valero et al. 2020) and in line with the surface velocity fluctuations of Arosquipa Nina et al. (2021). This is illustrated in Fig. 11, presenting their OF dimensionless streamwise fluctuations Tu_s obtained with two different setups, their dimensionless streamwise fluctuations Tu_{90} recorded with a dual-tip phase-detection probe in the aerated flow region (star symbols), and the OF dimensionless streamwise fluctuations Tu_s corresponding to the Hinze Dam Stage 3 stepped spillway.

The spanwise/transverse surface velocity fluctuations v_t' were significantly smaller than the streamwise fluctuations. In average across the spillway width, and immediately upstream of the inception region, the spanwise turbulence intensity Tu_t was about

$$\frac{Tu_t}{Tu_s} = \frac{\sqrt{\overline{v_t'^2}}}{\sqrt{\overline{v_s'^2}}} \approx 0.2 \tag{8}$$

Noteworthy, both Eqs. (7) and (8) applied to all three flood events (i.e., for $71.7 < Q < 334$ m^3/s and $2.3 \times 10^7 < \mathrm{Re} < 1.08 \times 10^8$). The finding implied a strong anisotropy of the free-surface turbulence (FST) in the nonaerated flow region, shortly prior to the inception of free-surface aeration. There, the FST anisotropy was linked to surface boils, divergence, foam lines, and convergence.

The present OF surface vorticity results showed low vorticity levels at the spillway water surface in the nonaerated flow region [Fig. 10(e)]. The vorticity magnitudes were much smaller than surface observations at river confluences (Lewis and Rhoads 2015). Several factors might explain the low values herein. First and foremost, the surface data set was recorded in the nonaerated flow region, where the turbulent boundary layer was partially developed. That is, the boundary layer turbulence had negligible impact on the water surface and the upper water column behave like a pseudoideal fluid flow. Low-level surface vorticity would be expected with the ungated gated spillway crest design. Second, the coarse spatial resolution of the OF data implied that the vorticity data were implicitly filtered and that the contribution of small-scale turbulence was not included. In Fig. 10(e), the OF spatial resolution was about 0.021–0.0525 m. That is, the present surface vorticity

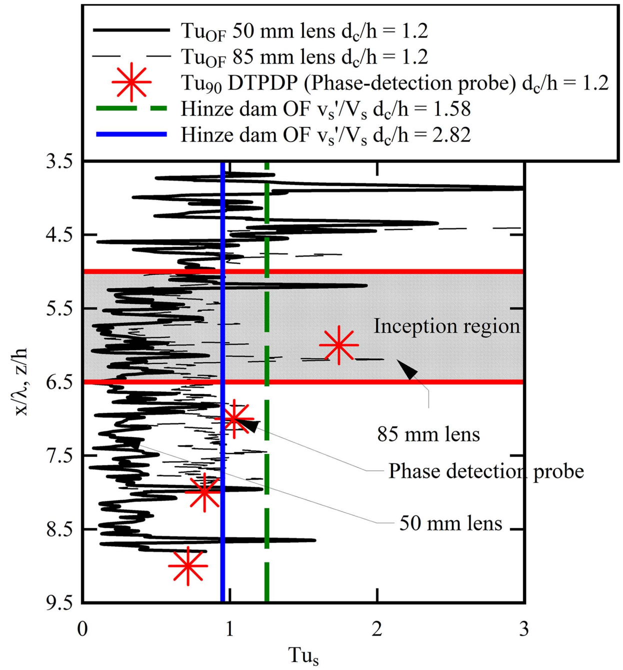

Fig. 11. Dimensionless longitudinal distribution of streamwise surface turbulence on the channel centerline, comparison between OF data at Hinze Dam Stage 3 stepped spillway on March 24, 2021 ($Q = 140$ m^3/s, $d_c/h = 1.58$, $\mathrm{Re} = 4.5 \times 10^7$) and March 31, 2017 ($Q = 334$ m^3/s, $d_c/h = 2.82$, $\mathrm{Re} = 10.9 \times 10^7$), OF data and phase-detection probe data at $y = \mathrm{Y}_{90}$ in a large-size laboratory stepped chute ($Q = 0.13$ m^3/s, $d_c/h = 1.2$, $\mathrm{Re} = 5.2 \times 10^5$). The laboratory OF measurements were conducted with a ultrahigh-speed camera (20,000 fps) and repeated with two lenses (50 and 85 mm). (Data from Arosquipa Nina et al. 2021.)

data characterized mostly large-scale turbulence and the present results in the nonaerated region indicated negligible large-scale surface turbulence there. The finding was consistent with the observations of well-organized longitudinal streaklines and surface ridges, starting slightly upstream of the spillway crest and extending up to the inception region [Fig. 3(a)].

Discussion

On Optical Flow Surface Velocity Data

The current OF technique may be affected by several possible types of issues. These might be linked to the light conditions, movie recording, processing, and postprocessing. Overall, the present experience showed a number of challenging issues with the application of OF to prototype stepped spillway flows. First, given the relatively large size of the pixel area, many scales of spillway flow motion may be smaller than the size of the interrogation area on which the OF analysis were performed; these scales are thus not resolved. A similar problem is known in large-scale image velocimetry (Fujita et al. 1998; Aberle et al. 2017) and one solution would be a much higher camera sensor resolution. Further, careful considerations must be given to some temporal scale issues when the data are recorded at relatively low frame rates like herein (see further discussion that follows). The large distance and, sometimes, a slight oblique angle between the camera lens axis and the surface flow may introduce lens and geometrical distortions.

The former may be avoided by using a prime lens with small distortion, and the latter may be removed using some geometrical transformation (Fujita et al. 1998).

In the specific context of the application of OF technique to high-velocity spillway flows at Hinze Dam Stage 3, the author's experience highlighted a number of key challenges:

- The OF data provided reasonably meaningful surface velocities in the nonaerated flow region upstream of the inception of free-surface aeration, albeit the fluctuating nature of the inception region affect the OF data immediately upstream. This was not initially expected, considering the past experience of Arosquipa Nina et al. (2021, 2022) with top view movies in laboratory.
- The OF data were physically meaningless in the air-water flow region. Several reasons may be put forward, including the limited temporal resolution and movie frame rate, coarse spatial resolution, lighting conditions, and weather conditions.
- The OF experience of the author suggests that both a faster movie frame rate and a larger video camera sensor would be required to achieve some meaningful temporal resolution in the air-water flow region. Since the OF tracks the changes in brightness due to reflectance difference associated with passages of air-water surface features, the time step between successive frames must be smaller than the time scales of these interfacial features (i.e., 1–50 ms). Further, at slow frame rates, the large changes in luminance between successive frames violate the fundamental assumption of brightness constancy. Thus, both arguments would warrant a minimum frame rate of 2,000–5,000 frames per second (fps). In addition, a larger video camera sensor would be warranted (e.g., 12,000 fps or more). Finally, it is also conceivable that different OF parameters should be chosen to suppress the noise and high frequency bias.
- The quality of the OF data was closely linked to the suitability of the observation point. Ideally, the camera should be placed perpendicular to the chute. At the Hinze Dam, this was not always possible because of local atmospheric conditions (i.e., mist and wind).
- The OF data quality was linked to the seeding of the free-surface flows. Generally, reasonable results were achieved in the nonaerated flow region with the presence of sediment-laden brown-colored waters. But the development of very long air-water streaks seemed to induce some errors, as seen in the OF data on March 31, 2017 (Chanson 2021).
- The video movie images were adversely affected by light reflections on free-surface instabilities, which could generate large fluctuations of the surface velocities.
- Optical conditions changed drastically between events, between successive days during the same flood event, and sometimes within one hour on a given day. These changes in light conditions could substantially impact the image quality.
- The video movies were recorded with different systems herein. The experience showed that, on a given day, the best image quality was achieved with professional dSLR cameras equipped with high-quality fast prime lenses. That is, single focal length lenses with large aperture and negligible lens distortion. The cameras were best positioned on a sturdy tripod, and the lens would ideally be equipped with a protective hood to minimize droplet deposition on the outer glass of the lens.
- The number of images per video movies should be ideally over 5,000 frames, with longer movies being desirable. Importantly, the camera should be fixed and immobile during the entire recording. For the whole movie recording, the natural lighting conditions should ideally remain constant, and the camera system must be protected from wind effects, mist, and spray.
- As previously stressed, the OF data quality is very strongly correlated to the quality of the lighting. While some preliminary testing is feasible in laboratory to improve the brightness, field observations rarely permit any in situ testing and this could be very challenging.

Overall, the present observations and discussion added to some earlier pertinent discussions (Shi et al. 2021; Arosquipa Nina et al. 2021).

Prototype Observations versus Laboratory (Visual) Observations

Prototype observations of stepped spillway overflow are rare, while laboratory (visual) observations have become very common. Yet, it is relevant to discuss the advantages and weaknesses of both types of observations and data sets (Table 3). Table 3 develops the pros and cons of both prototype and laboratory data sets.

First and foremost, the prototype observations are most important because they apply to the full-scale infrastructure. Despite a number of intrinsic difficulties listed in Table 3, they represent the ultimate data set. Quantitative prototype data are a fundamental requirement for the proper validation of both experimental and computational modeling. Roache (1998, p. 697) stressed: "*Validation has highest priority (to engineers and scientists) because nature is the final jury*." The prototype data set is *nature* (i.e., the *final jury*). Darrozes and Monavon (2014, p.12) further stated that "*the selection of the correct scales is a most critical point*," implying that the model scales (e.g., dimension and discharge) must be of the same order of magnitude as the full-scale dimensions

Table 3. Advantages and weaknesses of prototype and laboratory observations of stepped spillway overflow

	Prototype	Laboratory
Pros	• Full scale/Reference	• Controlled conditions (discharge, lighting, . . .) • Optical access (top, side, bottom) • Advanced instrumentation
Cons	• Free-surface observations (mostly) • Uncontrolled conditions (atmospheric, water discharge, lighting . . .) • Optical access (viewing point, parallax, distortion . . .) • Meteorological conditions (rainfall, wind, mist, fog . . .) • Safety (personnel, equipment) • Fast flowing waters	• Physical size of model • Limitations of hydrodynamic conditions (discharge, available head, Reynolds number, . . .) • Scale effects in small size models
Others	• Road access/closure during flood events • Photographic equipment (quality)	• Costs to build, operate, and maintain large physical model

$$L_m = O(L_p)$$
$$V_m = O(V_p)$$
$$Q_m = O(Q_p) \tag{9}$$

where L = characteristic length scale; V = characteristic velocity; Q = discharge; and subscript m and p = laboratory model and prototype, respectively. Practically, even in a large-size stepped chute model, Eq. (9) cannot be fulfilled.

On the other hand, a number of variables are uncontrolled during a prototype operation, while physical and optical accessibility might hamper any form of observations. High-quality field observations of stepped spillway overflow are very rare because they are difficult to conduct safely and accurately.

Conclusion

The Hinze Dam Stage 3 is equipped with a steep stepped chute controlled by an ungated ogee crest. Between 2013 and 2021, several overflow events were documented with detailed observations for six flow rates within $20.9\ \mathrm{m^3/s} < Q < 334\ \mathrm{m^3/s}$, corresponding to dimensionless discharges $0.44 < d_c/h < 2.82$ and Reynolds numbers ranging from 0.68×10^7 to 10.8×10^7. This study focused on the stepped spillway hydrodynamics with an emphasis on the skimming flow regime. Key results included the basic flow patterns, inception of free-surface aeration, and surface velocity field. Some uniquely novel aspects of the research included a series of systematic observations of a full-scale prototype stepped spillway, operating with a relatively wide range of unit discharges $1.71\ \mathrm{m^2/s} < q < 27.3\ \mathrm{m^2/s}$, by a renown expert using professional photographic equipment handled by the same photographer at a facility with excellent optical and physical access.

The main outcomes of the study are:

- For all investigated flow conditions, the skimming flow consisted of a nonaerated flow region followed by an air-water flow region with significant air entrainment. In the nonaerated flow region, a dense network of longitudinal surface streaklines was observed. The location of the inception of free-surface aeration was not a straight line, but a surface plane with some transient three-dimensional features.
- The location of and water depth at the inception of free-surface aeration were recorded and successfully compared to the literature. The comparison emphasized the needs for excellent optical access to record reliable and accurate prototype data.
- The free surface immediately upstream of the air entrainment inception region presented elongated air-water surface features. The high-resolution observations suggested a three-dimensional air entrapment process, induced by explosive interactions between elongated vortical structures generated by the invert and the free surface. A novel conceptual model of the entrapment mechanism was proposed, with five stages (Fig. 5).
- A robust OF technique was applied to video movies taken from a downstream observation platform facing the stepped chute. The OF data provided physically meaningful surface velocities in the nonaerated flow region upstream of the inception of free-surface aeration, with streamwise velocities close to ideal fluid flow predictions. In the vicinity of the inception region, the fluctuating nature of the interactions between turbulent structures and water surface adversely impacted on the OF results.
- Large streamwise surface velocity fluctuations were observed, while the spanwise surface velocity fluctuations were much smaller. That is, the data showed a strong anisotropy of the free-surface turbulence in the nonaerated flow region.
- The OF data outputs were meaningless in the air-water flow region, likely caused by a combination of limited temporal resolution and movie frame rate, coarse spatial resolution, and light and weather conditions.

In the last few decades, there has been a trend to work with larger physical models to minimize potential scale effects, especially for air-water spillway flows. A key question is: how big does a physical model, or CFD numerical model, need to be? Unless prototype data are collected at large Reynolds numbers, greater than 10^7, no one can answer this question. The present study is an attempt to provide field observations with Reynolds numbers ranging from 0.68×10^7 to 10.8×10^7, through the world's first successful detailed velocity measurements in a prototype stepped spillway. It is acknowledged that the current OF technique had limitations and could be affected by several possible types of errors. A better temporal and spatial resolution would be required to gain physically meaningful outputs in the air-water flow region. The OF data quality was strongly correlated to the quality of camera sensor and optics.

Data Availability Statement

Some or all data, models, or code that support the findings of this study are available from the corresponding author upon reasonable request. Further information is reported in Chanson (2021).

Acknowledgments

The author wants to thank the reviewers, Dr. Gangfu Zhang (AECOM, Australia) and Dr. John Macintosh (Water Solutions, Australia), for the detailed comments on the report and very helpful suggestions. He further thanks Professor Jorge Matos for constructive exchanges. The author acknowledges Mr. Barton Maher (Seqwater) for providing technical details of the Hinze Dam Stage 3, as well as all the Seqwater personnel who assisted the author during technical visits. He also thanks Mr. Rui (Ray) Shi (The University of Queensland) for his technical advice on the optical flow calculations. Professor Fabian Bombardelli (University of California Davis, USA) is thanked for his encouragement. The financial support of the University of Queensland, School of Civil Engineering is acknowledged.

Notation

The following symbols are used in this paper:

B = channel width (m): $B = 12.25$ m in low level section of the Hinze Dam Stage 3 stepped spillway;
D_H = hydraulic diameter (m);
d = water depth (m) measured normal to the pseudoinvert formed by the step edges;
d_c = critical flow depth (m);
d_I = water depth (m) at inception region of free-surface aeration, measured based upon the water level on the training walls at Hinze Dam stepped spillway;
F = characteristic frequency (Hz) in surface scar generation rate fluctuations;
F^* = Froude number defined in terms of the gravity component in the flow direction and step cavity depth:
$$F_* = (q/\sqrt{g \times \sin\theta \times k^3})$$
$$= (1/\sqrt{\sin\theta \times (\cos\theta)^3}) \times (d_c/h)^{3/2};$$

g = gravity acceleration (m/s^2): $g = 9.794$ m/s^2 in Brisbane, Australia;
H_1 = upstream head above crest invert (m);
h = vertical step height (m);
L = length scale (m);
L_I = position (m) of inception region of free-surface aeration measured from downstream end of the chute crest;
l_t = average transverse spacing (m) between elongated air-water surface features in vicinity of the inception region;
Q = water discharge (m^3/s);
q = water discharge per unit width (m^2/s): $q = Q/B$;
Re = Reynolds number defined in terms of mean velocity and hydraulic diameter: $\mathrm{Re} = \rho \times [(V_{mean} \times D_H)/\mu]$;
St = Strouhal number;
s = streamwise coordinate (m);
Tu_s = streamwise turbulence intensity: $Tu_s = (\sqrt{v_s'^2}/\overline{V_s})$;
Tu_t = spanwise turbulence intensity: $Tu_t = (\sqrt{v_t'^2}/\overline{V_s})$;
t = time (s);
V = velocity (m/s);
$V_{\max}$ = potential flow velocity (m/s) (i.e., ideal flow velocity for a given total head);
V_s = streamwise surface velocity component (m/s) positive downstream and measured tangential to free surface;
$\overline{V_s}$ = streamwise surface velocity component (m/s) averaged across chute width;
V_t = transverse surface velocity component (m/s) positive toward left training wall;
v_s' = standard deviation of streamwise velocity component (m/s);
v_t' = standard deviation of transverse/spanwise velocity component (m/s);
y = transverse distance (m) measured from the right training wall and positive toward left training wall;
z = 1–vertical elevation (m);
z_{crest} = crest invert elevation (m);
θ = angle between pseudobottom formed by step edges and horizontal; and
ω = surface vorticity (1/s).

Subscript

c = critical flow conditions;
I = inception conditions;
m = model property;
p = prototype property;
s = streamwise component; and
t = spanwise/transverse component.

References

Aberle, J., C. Rennie, D. M. Admiraal, and M. Muste. 2017. *Experimental hydraulics: Methods, instrumentation, data processing and management. Vol. II. Instrumentation and measurement techniques*. IAHR Monograph 408. New York: Taylor and Francis.

Amador, A., M. Sanchez-Juny, and J. Dolz. 2006. "Characterization of the nonaerated flow region in a stepped spillway by PIV." *J. Fluids Eng.* 128 (6): 1266–1273. https://doi.org/10.1115/1.2354529.

Anwar, H. O. 1994. "Self-aerated flows on chutes and spillways—Discussion." *J. Hydraul. Eng.* 120 (6): 778–779. https://doi.org/10.1061/(ASCE)0733-9429(1994)120:6(778).

Arosquipa Nina, Y., R. Shi, D. Wüthrich, and H. Chanson. 2021. *Intrusive and non-intrusive air-water measurements on stepped spillways with inclined steps: A physical study on air entrainment and energy dissipation*. Hydraulic Model Rep. No. CH121/21. Brisbane, Australia: School of Civil Engineering, Univ. of Queensland.

Arosquipa Nina, Y., R. Shi, D. Wüthrich, and H. Chanson. 2022. "Intrusive and non-intrusive two-phase air-water measurements on stepped spillways: A physical study." *Exp. Therm. Fluid Sci.* 131 (Feb): 110545. https://doi.org/10.1016/j.expthermflusci.2021.110545.

Barua, D. K., and K. H. Rahman. 1998. "Some aspects of turbulent flow structure in large alluvial rivers." *J. Hydraul. Res.* 36 (2): 235–252. https://doi.org/10.1080/00221689809498635.

Best, J. 2005. "The fluid dynamics of river dunes: A review and some future research directions." *J. Geophys. Res.* 110 (Dec): 21. https://doi.org/10.1029/2004JF000218.

Boes, R. M., and W. H. Hager. 2003. "Two-phase flow characteristics of stepped spillways." *J. Hydraul. Eng.* 129 (9): 661–670. https://doi.org/10.1061/(ASCE)0733-9429(2003)129:9(661).

Bombardelli, F. A., I. Meireles, and J. Matos. 2011. "Laboratory measurements and multi-block numerical simulations of the mean flow and turbulence in the non-aerated skimming flow region of steep stepped spillways." *Environ. Fluid Mech.* 11 (3): 263–288. https://doi.org/10.1007/s10652-010-9188-6.

Brocchini, M. 2002. "Free surface boundary conditions at a bubbly/weakly splashing air-water interface." *Phys. Fluids* 14 (6): 1834–1840. https://doi.org/10.1063/1.1475998.

Brocchini, M., and D. H. Peregrine. 2001. "The dynamics of strong turbulence at free surfaces. Part 1. Description." *J. Fluid Mech.* 449 (Dec): 225–254. https://doi.org/10.1017/S0022112001006012.

Bung, D. B., and D. Valero. 2016. "Optical flow estimation in aerated flows." *J. Hydraul. Res.* 54 (5): 575–580. https://doi.org/10.1080/00221686.2016.1173600.

Chamani, M. R. 2000. "Air inception in skimming flow regime over stepped spillways." In *Proc., Int. Workshop on Hydraulics of Stepped Spillways*, edited by H. E. Minor and W. H. Hager, 61–67. Zürich, Switzerland: Balkema Publication.

Chanson, H. 1994. "Hydraulics of skimming flows over stepped channels and spillways." *J. Hydraul. Res.* 32 (3): 445–460. https://doi.org/10.1080/00221689409498745.

Chanson, H. 1995. *Hydraulic design of stepped cascades, channels, weirs and spillways*, 292. Oxford, UK: Pergamon.

Chanson, H. 1997. *Air bubble entrainment in free-surface turbulent shear flows*, 401. London: Academic Press.

Chanson, H. 2001. *The hydraulics of stepped chutes and spillways*. Lisse, Netherlands: Balkema.

Chanson, H. 2004. *The hydraulics of open channel flow: An introduction*. 2nd ed. Oxford, UK: Butterworth-Heinemann.

Chanson, H. 2009. "Turbulent air-water flows in hydraulic structures: Dynamic similarity and scale effects." *Environ. Fluid Mech.* 9 (2): 125–142. https://doi.org/10.1007/s10652-008-9078-3.

Chanson, H. 2013. "Interactions between a developing boundary layer and the free-surface on a stepped spillway: Hinze Dam spillway operation in January 2013." In *Proc., 8th Int. Conf. on Multiphase Flow ICMF 2013*. Jeju, Korea: International Convention Center Jeju.

Chanson, H. 2021. *Stepped spillway prototype operation, spillway flow and air entrainment: The Hinze Dam, Australia*. Hydraulic Model Rep. No. CH123/21. Brisbane, Australia: School of Civil Engineering, Univ. of Queensland.

Chanson, H., D. Bung, and J. Matos. 2015. "Stepped spillways and cascades." In *Energy dissipation in hydraulic structures*, edited by H. Chanson, 45–64. Leiden, Netherlands: CRC Press, Taylor & Francis Group.

Chanson, H., X. Leng, and H. Wang. 2021. "Challenging hydraulic structures of the 21st century—From bubbles, transient turbulence to fish passage." *J. Hydraul. Res.* 59 (1): 21–35. https://doi.org/10.1080/00221686.2020.1871429.

Chanson, H., Y. Yasuda, and I. Ohtsu. 2002. "Flow resistance in skimming flows and its modeling." *Can. J. Civ. Eng.* 29 (6): 809–819. https://doi.org/10.1139/l02-083.

Darrozes, S. S., and A. Monavon. 2014. *Analyse Phénoménologique des Ecoulements. Comment traiter un Problème de Mécanique des Fluides avant de résoudre les Equations. [Phenomenological analysis of flows.*

J. Hydraul. Eng., 2022, 148(11): 05022004

How to solve a fluid mechanics problem before solving the equations], 480. [In French.] Lausanne, Switzerland: Presses Polytechniques et Universitaires Romandes.

Ervine, D. A. 1998. "Air entrainment in hydraulic structures: A review." *Proc. Inst. Civ. Eng. Water Marit. Energy* 130 (3): 142–153. https://doi.org/10.1680/iwtme.1998.30973.

Ervine, D. A., and H. T. Falvey. 1987. "Behaviour of turbulent water jets in the atmosphere and in plunge pools." *Proc. Inst. Civ. Eng.* 83 (1): 295–314. https://doi.org/10.1680/iicep.1987.353.

Felder, S., and H. Chanson. 2014. "Air–water flows and free-surface profiles on a non-uniform stepped chute." *J. Hydraul. Res.* 52 (2): 253–263. https://doi.org/10.1080/00221686.2013.841780.

Fujita, I., M. Muste, and A. Kruger. 1998. "Large-scale particle image velocimetry for flow analysis in hydraulic engineering applications." *J. Hydraul. Res.* 36 (3): 397–414. https://doi.org/10.1080/00221689809498626.

Galanti, B., and P. L. Sulem. 1991. "Inverse cascades in three-dimensional anisotropic flows lacking parity invariance." *Phys. Fluids A* 3 (7): 1778–1784. https://doi.org/10.1063/1.857958.

Halbronn, G. 1952. "Etude de la Mise en Régime des Ecoulements sur les Ouvrages à Forte Pente. Applications au problème de l'Entraînement d'Air." [Study of the setting up of the flow regime on high gradient structures. Application to air entrainment problem]. [In French.] *Jl La Houille Blanche* 39 (1): 21–40. https://doi.org/10.1051/lhb/1952018.

Hino, M. 1961. "On the mechanism of self-aerated flow on steep slope channels. Applications of the statistical theory of turbulence." In *Proc., 9th IAHR Congress*, 123–132. Beijing: Spain Water and IAHR.

Horn, B. K., and B. G. Schunck. 1981. "Determining optical flow." *Artif. Intell.* 17 (1–3): 185–203. https://doi.org/10.1016/0004-3702(81)90024-2.

Imamoto, H., and T. Ishigaki. 1986. "Visualization of longitudinal eddies in an open channel flow." In *Proc., 4th Int. Symp. on Flow Visualization*, 333–337. Washington, DC: Association Nationale de la Recherche Technique.

Jackson, R. G. 1975. "A depositional model of point bars in the lower Wabash River." Ph.D. thesis, Dept. of Geology, Illinois Univ.

Keller, R. J., and A. K. Rastogi. 1975. "Prediction of flow development on spillways." *J. Hydraul. Div.* 101 (9): 1171–1184. https://doi.org/10.1061/JYCEAJ.0004414.

Korchokha, Y. M. 1968. "Investigation of the dune movement of sediments on the Polomet' River." *Soc. Hydrol.* 6: 541–559.

Lane, E. W. 1939. "Entrainment of air in swiftly flowing water. Observations of the flow over spillways yield conclusions of interest to hydraulic engineers." *Civ. Eng.* 2 (Feb): 89–91.

Levi, E. 1965. "Longitudinal streaking in liquid currents." *J. Hydraul. Res.* 3 (2): 25–39. https://doi.org/10.1080/00221686509500083.

Levi, E. 1983. "A universal Strouhal law." *J. Eng. Mech.* 109 (3): 718–727. https://doi.org/10.1061/(ASCE)0733-9399(1983)109:3(718).

Lewis, Q. W., and B. L. Rhoads. 2015. "Resolving two-dimensional flow structure in rivers using large-scale particle image velocimetry: An example from a stream confluence." *Water Resour. Res.* 51 (10): 7977–7994. https://doi.org/10.1002/2015WR017783.

Liu, T., and L. Shen. 2008. "Fluid flow and optical flow." *J. Fluid Mech.* 614 (Nov): 253–291. https://doi.org/10.1017/S0022112008003273.

Lubin, P., and H. Chanson. 2017. "Are breaking waves, bores, surges and jumps the same flow?" *Environ. Fluid Mech.* 17 (1): 47–77. https://doi.org/10.1007/s10652-016-9475-y.

Novak, P., A. I. B. Moffat, C. Nalluri, and R. Narayanan. 1996. *Hydraulic structures*. 2nd ed., 599. London, UK: E & FN Spon.

Ohtsu, I., and Y. Yasuda. 1997. "Characteristics of flow conditions on stepped channels." In *Proc., 27th IAHR Biennal Congress*, 583–588. Reston, VA: EWRI-ASCE.

Phillips, M., and K. Ridette. 2007. "Computational fluid dynamics models and physical hydraulic modeling—Do we need both? The design of the Hinze Dam Stage 3." In *Proc., 2007 NZSOLD/ANCOLD Conf.*, 8. Wellington, New Zealand: Society of Large Dams.

Rajaratnam, N. 1990. "Skimming flow in stepped spillways." *J. Hydraul. Eng.* 116 (4): 587–591. https://doi.org/10.1061/(ASCE)0733-9429(1990)116:4(587).

Roache, R. L. 1998. *Verification and validation in computational science and engineering*, 446. Albuquerque, NM: Hermosa Publishers.

Robinson, S. K. 1991. "Coherent motions in the turbulent boundary layer." *Annu. Rev. Fluid Mech.* 23 (1): 601–639. https://doi.org/10.1146/annurev.fl.23.010191.003125.

Roshko, A. 1954. *On the drag and shedding frequency of two-dimensional bluff bodies*. NACA Technical Note 3169, 30. Kitty Hawk, NC: National Advisory Committee for Aeronautics.

Sarpakaya, T. 1996. "Vorticity, free surface, and surfactants." *Annu. Rev. Fluid Mech.* 28 (1): 83–128. https://doi.org/10.1146/annurev.fl.28.010196.000503.

SEQWATER. 2011a. *Spillway. General arrangement*. Brisbane, Australia: Seqwater.

SEQWATER. 2011b. *Spillway. Main spillway. General plan*. Brisbane, Australia: Seqwater.

SEQWATER. 2011c. *Spillway. Main spillway. High level section and details. Sheet 1 of 2*. Brisbane, Australia: Seqwater.

SEQWATER. 2011d. *Spillway. Main spillway. High level section and details. Sheet 2 of 2*. Brisbane, Australia: Seqwater.

SEQWATER. 2011e. *Spillway. Main spillway. Low level section and details*. Brisbane, Australia: Seqwater.

SEQWATER. 2011f. *Spillway. Main spillway. Low level training walls*. Brisbane, Australia: Seqwater.

Shi, R., D. Wüthrich, and H. Chanson. 2021. "*Air-water characteristics of a breaking bore roller Part II: Air-water flow properties*. Hydraulic Model Rep. No. CH118/20. Brisbane, Australia: School of Civil Engineering, Univ. of Queensland.

Sorensen, R. M. 1985. "Stepped spillway hydraulic model investigation." *J. Hydraul. Eng.* 111 (12): 1461–1472. https://doi.org/10.1061/(ASCE)0733-9429(1985)111:12(1461).

Theodorsen, T. 1952. "Mechanisms of turbulence." In *Proc., 2nd Midwestern Conf. on Fluid Mechanics*, 1–18. Columbus, OH: Ohio State Univ.

Toombes, L., and H. Chanson. 2007. "Surface waves and roughness in self-aerated supercritical flow." *Environ. Fluid Mech.* 7 (3): 259–270. https://doi.org/10.1007/s10652-007-9022-y.

Toro, J. P., F. A. Bombardelli, and J. Paik. 2017. "Detached Eddy simulation of the nonaerated skimming flow over a stepped spillway." *J. Hydraul. Eng.* 143 (9): 04017032. https://doi.org/10.1061/(ASCE)HY.1943-7900.0001322.

USBR. 1965. *Design of small dams*. 1st ed. Denver: Bureau of Reclamation, US Dept. of the Interior.

Valero, D., and D. B. Bung. 2018. "Reformulating self-aeration in hydraulic structures: Turbulent growth of free surface perturbations leading to air entrainment." *Int. J. Multiphase Flow* 100 (Mar): 127–142. https://doi.org/10.1016/j.ijmultiphaseflow.2017.12.011.

Valero, D., H. Chanson, and D. B. Bung. 2020. "Robust estimators for free surface turbulence characterization: A stepped spillway application." *Flow Meas. Instrum.* 76 (Dec): 1014809. https://doi.org/10.1016/j.flowmeasinst.2020.101809.

Vischer, D., and W. H. Hager. 1998. *Dam hydraulics*, 316. Chichester, UK: Wiley.

Wood, I. R. 1985. "Air water flows." In *Proc., 21st IAHR Congress*, 18–29. Beijing: Spain Water and IAHR.

Wood, I. R. 1991. "Air entrainment in free-surface flows." In *IAHR hydraulic structures design manual no. 4, Hydraulic design considerations*, 149. Rotterdam, Netherlands: A.A. Balkema.

Wood, I. R., P. Ackers, and J. Loveless. 1983. "General method for critical point on spillways." *J. Hydraul. Eng.* 109 (2): 308–312. https://doi.org/10.1061/(ASCE)0733-9429(1983)109:2(308).

Zabaleta, F., and F. A. Bombardelli. 2020. "Eddy-resolving simulation of flows over macro-roughness." In *Proc., RiverFlow2020*, 1293–1299. Boca Raton, FL: CRC Press.

Zabaleta, F., F. A. Bombardelli, and J. P. Toro. 2020. "Towards an understanding of the mechanisms leading to air entrainment in the skimming flow over stepped spillways." *Environ. Fluid Mech.* 20 (2): 375–392. https://doi.org/10.1007/s10652-019-09729-2.

Zhang, G. 2017. "Free-surface aeration, turbulence, and energy dissipation on stepped chutes with triangular steps, chamfered steps, and partially blocked step cavities." Ph.D. thesis, Univ. of Queensland, School of Civil Engineering.

Zhang, G., and H. Chanson. 2016a. "Hydraulics of the developing flow region of stepped spillways. I: Physical modeling and boundary layer development." *J. Hydraul. Eng.* 142 (7): 04016015. https://doi.org/10.1061/(ASCE)HY.1943-7900.0001138.

Zhang, G., and H. Chanson. 2016b. "Hydraulics of the developing flow region of stepped spillways. II: Pressure and velocity fields." *J. Hydraul. Eng.* 142 (7): 04016016. https://doi.org/10.1061/(ASCE)HY.1943-7900.0001136.

Zhang, G., and H. Chanson. 2018. "Application of local optical flow methods to high-velocity free-surface flows: Validation and application to stepped chutes." *Exp. Therm Fluid Sci.* 90 (Jan): 186–199. https://doi.org/10.1016/j.expthermflusci.2017.09.010.